Net Efficiency-Equipment Trade-offs in PWR-SMR Rankine Cycles: Impacts of Steam-Generator Pressure and Temperature

Gyudong Kim ^a, Jeong Ik Lee ^{a*}
^aDepartment of Nuclear and Quantum Engineering, KAIST 373-1, Guseong-dong, Yuseong-gu, Daejeon, 305-701, Republic of Korea

*Corresponding author: jeongiklee@kaist.ac.kr

*Keywords: Small modular reactor(SMR), Rankine cycle, Equipment sizing, Steam generator condition, Net efficiency

1. Introduction

Small modular reactors (SMRs) are gaining prominence as a compact, factory-fabricable nuclear system that can deliver low-carbon electricity while reducing siting and deployment constraints; their modularity and smaller footprints are key advantages highlighted in recent overviews [1,2].

Among pressurized-water SMRs (PWR-SMRs), many integral concepts adopt once-through, helical-coil steam generators (SGs) to reduce inventory and simplify systems—an approach exemplified by NuScale and SMART. NuScale's integral module employs interleaved helical-coil SG bundles within the vessel, and its published main-steam supply pressure is ≈3.5 MPa with ≈300 °C steam, i.e., at the lower end of conventional PWR secondary pressures. SMART likewise uses modular once-through helical SGs and targets a mainsteam pressure of ≈5.2 MPa with steam temperature ≈298 °C. For comparison at higher pressure in the same technology lineage, Westinghouse's AP300 is derived from the AP1000; the AP1000 main steam is reported around 5.5 MPa, indicating that contemporary lightwater designs span roughly 3-6 MPa on the secondary side. The difference in various designs motivate the mapping of efficiency and equipment implications across SG outlet pressure and SG inlet temperature [3-6].

From a thermodynamic standpoint, higher steam pressure and temperature generally improve Rankine-cycle efficiency; however, they also reshape where (and how much) feedwater heating is performed. With fixed terminal approaches in the heaters, the log-mean temperature difference (LMTD) is effectively prescribed, so the required overall heat-transfer conductance UA scales with the duty. Since the overall coefficient U is bounded by allowable coolant velocities, materials, and fouling, increases in UA typically imply increases in heat-transfer area A and thus larger, costlier heaters—a well-established linkage in heat-exchanger design and costing practice. In other words, UA is a practical proxy for heater size and capital cost [7-10].

Using the KAIST-CCD cycle analysis tool, this study quantifies—on a common footing—how steamgenerator (SG) outlet pressure (\approx 3–6 MPa) and SG inlet temperature (\approx 150–250 °C) jointly affect (i) net cycle

efficiency, (ii) high- and low-pressure turbine behavior, including the onset of wet-steam expansion, and (iii) the aggregate overall heat-transfer individual and conductance (UA) of closed feedwater heaters. It is found that moving to higher pressure delivers a modest gain in net efficiency but requires larger heater UA (and necessitate additional moisture-management hardware if turbine wetness increases), whereas lowering pressure reduces UA and implied heater size at the cost of efficiency. Importantly, the UA trend with pressure is not strictly monotonic—a localized increase appears in the mid-pressure region—so simply reducing pressure does not guarantee smaller heaters. These results provide design guidance for selecting SG pressure and SG inlet temperature that balance efficiency with equipment size (and cost) for grid-responsive PWR-SMRs. [11-13].

2. Methods

To assess how heat-exchanger capacity and efficiency depend on steam-generator (SG) conditions, the SG outlet pressure was varied from 3000 to $6000 \, \mathrm{kPa}$ and the SG inlet temperature from 150 to 250 °C and quantified the resulting changes in overall heat-transfer conductance (UA) and net cycle efficiency.

2.1 Plant Configuration and Boundary Conditions (500 MW_{th} PWR-based SMR)

The secondary-side steam cycle analyzed here follows a widely adopted PWR configuration and was sized for a preliminary 500 MW_{th} SMR study. Table 1 summarizes the cycle boundary conditions and performance constraints, and Fig. 1 shows the equipment layout. In addition, Fig. 2 shows the SG operating domain considered (3–6 MPa outlet pressure and 150–250 °C inlet temperature) together with the saturation temperature at the SG inlet pressure. The configuration comprises a steam generator, condenser, high- and low-pressure turbines, a moisture separator, three closed feedwater heaters, a deaerator (open heater), and two feedwater pumps.

All component models were evaluated under the specified operating conditions. The condenser was constrained to meet the prescribed outlet pressure and inlet temperature, and the steam-generator duty was set

to transfer the full 500 MW_{th} of heat to the feedwater. Fixed fractional pressure drops were imposed as follows: 3 % on all heating paths (feedwater and steam through the steam generator, reheater, and feedwater heaters) and 2 % on cooling paths (condensate and extraction drains). Turbine expansions were modeled with an isentropic efficiency of 90 % for expansions initiated at saturatedvapor conditions (quality x=1). The moisture separator was assumed to achieve complete phase separation. All three feedwater heaters were treated as closed units, with a terminal temperature difference of 5 °F and a draincooler approach of 10 °F applied uniformly [14]. The deaerator was sized to provide the required thermal lift but was not modeled for gas-stripping performance. Both feedwater pumps were assigned an isentropic efficiency of 80 %.

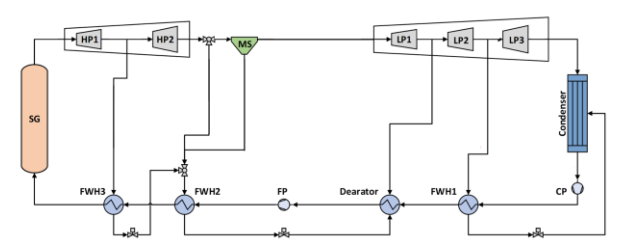


Fig. 1. Conceptual diagram of steam cycle of PWR-SMR power plants.

Table I: cycle conditions and constraints of the steam cycle.

Input variable	Value
SG outlet temperature [°C]	315
SG outlet pressure [kPa]	3,000 to 6,000
SG inlet temperature [°C]	150 to 250
Thermal output [MW]	500
Turbine efficiency [%]	90
Pump efficiency [%]	80
Generator efficiency [%]	96
Condenser pressure [kPa]	7.38
Feedwater heater TTD [°C]	2.78
Feedwater heater DCA [°C]	8.33
Hot side pressure drop [%]	3% of inlet
Cold side pressure drop [%]	2% of inlet

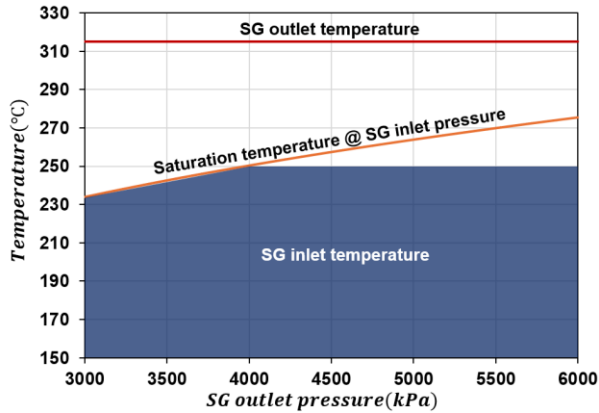


Fig. 2. Study Inputs—SG Outlet Pressure vs. Outlet Temperature, with Inlet-Temperature Domain and Saturation

at Inlet Pressure

2.2 Turbine Expansion and Wet-Steam Efficiency Penalties

Since the steam-generator (SG) inlet temperature is prescribed as an input variable, enforcing the terminal temperature difference (TTD) at Feedwater Heater #3 (FWH3) fixes the saturation state at the exit of the first high-pressure turbine (HPT) stage:

$$\begin{split} T_{sat, \text{HPT1,out}} &= T_{\text{SG,in}} + TTD, \\ P_{\text{HPT1,out}} &= P_{sat} @ \left(T_{sat, \text{HPT1,out}} \right) \end{split}$$

Given $P_{\mathrm{HPT1,out}}$, the overall HPT pressure ratio follows as

$$HPT PR = \left(\frac{P_{\text{HPT,in}}}{P_{\text{HPT1,out}}}\right)^2$$
.

The low-pressure turbine (LPT) pressure ratio is then determined by the HPT exhaust and condenser pressures:

$$LPT PR = \frac{P_{\text{HPT,out}}}{P_{\text{cond}}}.$$

Consequently, variations in SG outlet pressure and SG inlet temperature shift the turbine pressure ratios and, therefore, the wetness trajectories through both HPT and LPT. For superheated steam, an isentropic efficiency of 90% is assumed for both turbines; however, once expansion enters the wet-steam region, supersaturation and moisture carry-over induce additional losses that reduce stage efficiency. To account for these effects, Cotton's empirical correlations are applied to impose efficiency penalties as a function of stage-averaged moisture content. The relationship between internal average moisture and efficiency loss is shown in Fig. 3, and the corresponding calculation workflow for turbine efficiency is summarized in Fig. 4 [15].

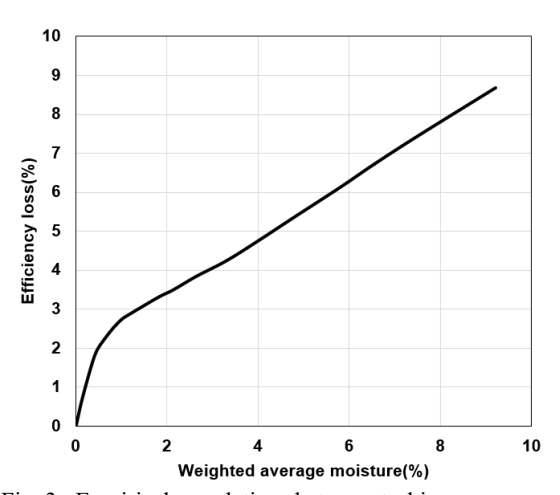


Fig. 3. Empirical correlations between turbine average moisture and loss in turbine isentropic efficiency[15].

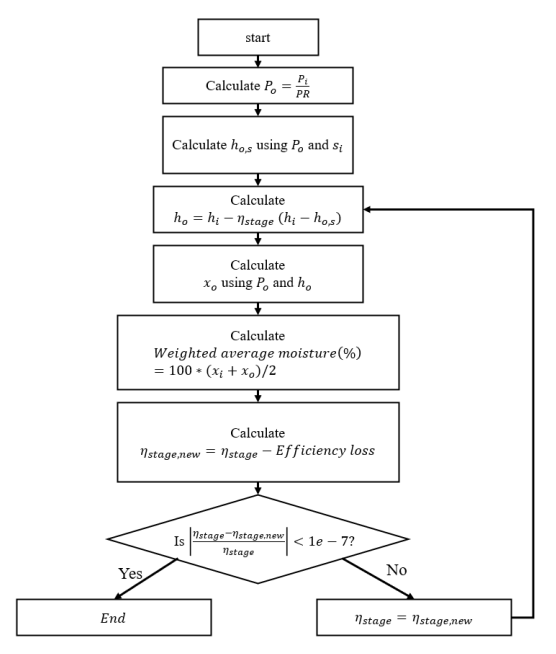


Fig. 4. Flowchart of turbine stage isentropic efficiency calculation using weighted average moisture fraction.

2.3 TTD/DCA and LMTD-UA Formulation

To meet the fixed TTD and DCA targets at each feedwater heater, the turbine extraction-line flow rates were adjusted until the cycle heat balance was met.

The overall heat-transfer conductance (UA) is obtained from the heat duty (Q) and the log-mean temperature difference (LMTD):

$$UA = Q/LMTD$$

Since the terminal temperature difference (TTD) and the drain-cooler approach (DCA) are held fixed for all feedwater heaters, the LMTD is insensitive to changes in steam-generator (SG) outlet pressure and SG inlet temperature. The LMTD is evaluated as:

$$LMTD = \frac{DCA - TTD}{ln(DCA/TTD)}$$

consistent with a two-terminal exchanger whose end temperature differences are $\Delta T_1 = DCA$ and $\Delta T_2 = TTD$. Using this LMTD, the UA of each feedwater heater is then computed.

3. Results and Discussion

3.1 T-s Diagrams: Effects of SG Outlet Pressure and Inlet Temperature on Expansion Path and Wetness

Fig. 5 presents temperature–entropy (T–s) diagrams for steam-generator (SG) outlet pressures of 3,000(Fig. 5a) and 6,000 kPa(Fig. 5b) at SG inlet temperatures of $150 \,^{\circ}$ C ("low") and $230 \,^{\circ}$ C ("high"). The upper bound of

230 °C for the 3,000 kPa case is imposed to prevent boiling of the SG inlet feedwater and to enable a consistent comparison.

At 3,000 kPa, a lower SG inlet temperature increases the high-pressure turbine (HPT) pressure ratio (PR), driving the expansion to cross into the wet-steam region by the HPT exit. The moisture separator (MS) then removes entrained liquid before the flow enters the low-pressure turbine (LPT). In contrast, at the higher SG inlet temperature the reduced HPT PR keeps the HPT exhaust superheated, rendering the MS effectively inactive. Under 3,000 kPa conditions, the MS-induced rise in steam quality at low SG inlet temperature can yield a net improvement in turbine efficiency.

At 6,000 kPa, the higher SG outlet pressure shifts the expansion toward earlier condensation, so the wet-steam region is traversed over a longer portion of the path than at 3,000 kPa; moreover, the HPT exhaust enters the two-phase region for both low and high SG inlet temperatures. These differences in the turbine internal steam state with SG inlet temperature and outlet pressure translate into differences in the condition of extraction steam admitted to the high-temperature sections of the feedwater heaters and are therefore expected to affect their required overall heat-transfer conductance (UA).

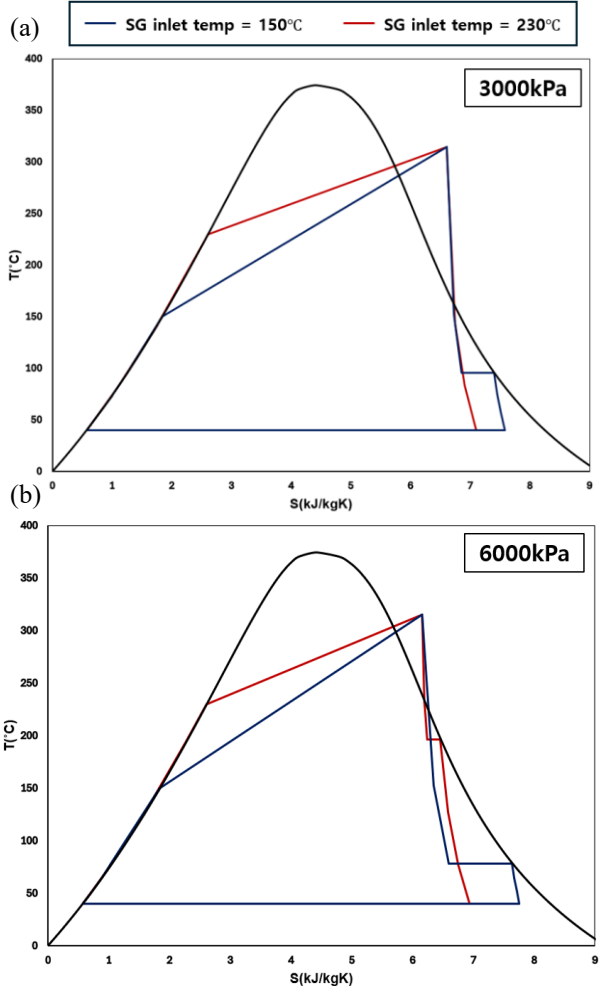


Fig. 5. T-s diagrams illustrating the effect of SG pressure ((a)

for 3000kPa, (b) for 6000kPa) and inlet temperature (150 and 230 $^{\circ}\mathrm{C})$

3.2. Effect of SG Outlet Pressure and Inlet Temperature on Feedwater-Heater UA

Fig. 6a-c plots the overall heat-transfer conductance (UA) of each closed feedwater heater (FWH1–FWH3) versus steam-generator (SG) outlet pressure (3,000–6,000 kPa) and SG inlet temperature (150–250 °C), and Fig. 6d reports the total UA (FWH1+FWH2+FWH3). With the terminal temperature difference (TTD) and drain-cooler approach held fixed, the log-mean temperature difference is invariant, so changes in UA directly reflect changes in heater duty. FWH1 and FWH2 show a monotonic increase in UA with both higher SG inlet temperature and higher SG outlet pressure, indicating that a larger share of the feedwater enthalpy rise is supplied upstream under hotter and higher-pressure conditions.

In contrast, FWH3 attains its largest UA at high pressure and low SG inlet temperature: lowering the SG inlet temperature (while enforcing the FWH3 TTD) requires a higher high-pressure-turbine pressure ratio, which reduces the HPT exhaust pressure, depresses the FWH2 outlet feedwater temperature, and thereby increases the thermal lift and duty demanded of FWH3. Despite this opposing trend at FWH3, the aggregate is dominated by FWH2; consequently, the total UA increases with SG inlet temperature and with SG outlet pressure.

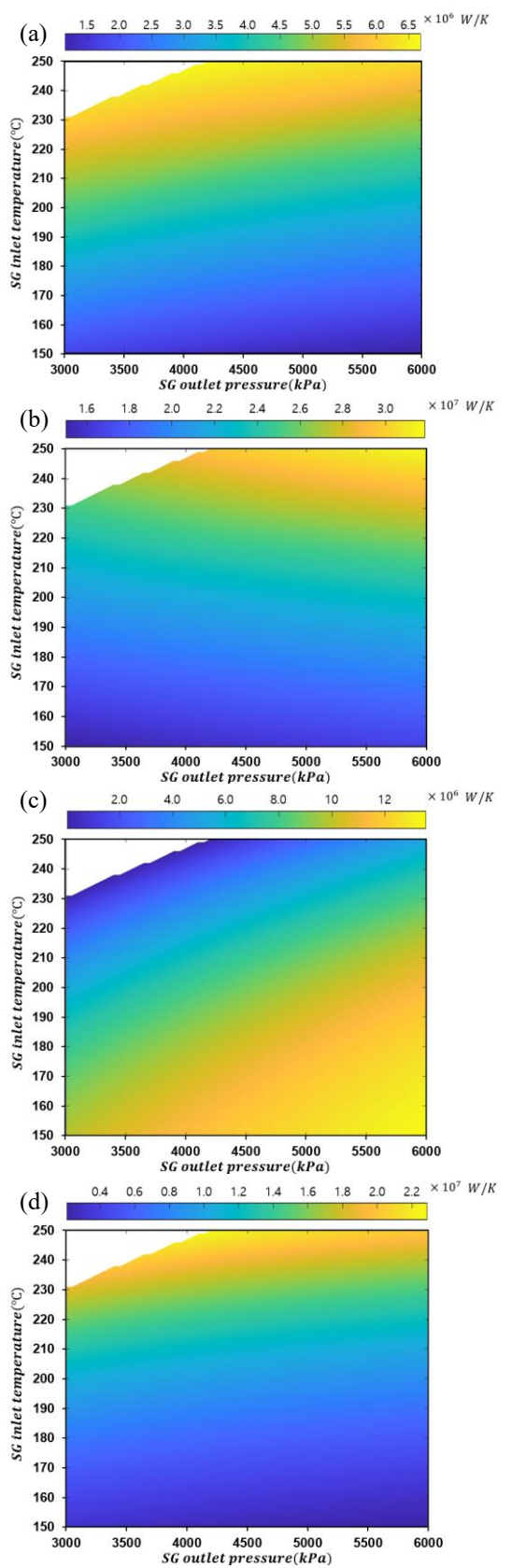


Fig. 6. UA maps for FWH1–FWH3(a-c) and total UA(d) as functions of SG pressure and inlet temperature.

3.3 Net Efficiency vs. SG Conditions and UA Trade-off Along the Optimal Path

Fig. 7 maps the net cycle efficiency as a function of steam-generator (SG) outlet pressure (3,000–6,000 kPa) and SG inlet temperature (150–230 °C), with a red dashed "best-efficiency line" tracing the locus of optimal operating points.

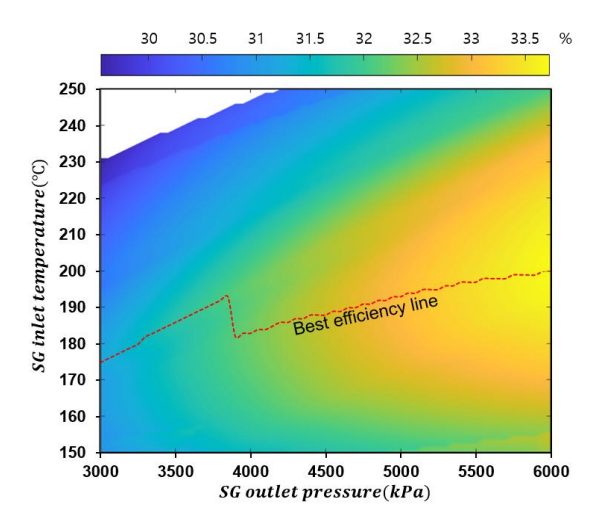


Fig. 7. Net efficiency map across SG pressure (3–6 MPa) and inlet temperature (150–230 °C) with best-efficiency line

Fig. 8a shows the corresponding high-pressure-turbine (HPT) isentropic efficiency, overlaid with "wet-steam lines" that mark the onset of two-phase expansion at the exits of HPT stage 1 and stage 2; efficiency rises toward higher temperature and higher pressure but drops sharply once the expansion path crosses into the wet region. Fig. 8b presents the low-pressure-turbine (LPT) efficiency, which varies more modestly since most of the LPT domain lies in the wet-steam region; a general trend of higher efficiency at higher pressure and lower SG inlet temperature is observed.

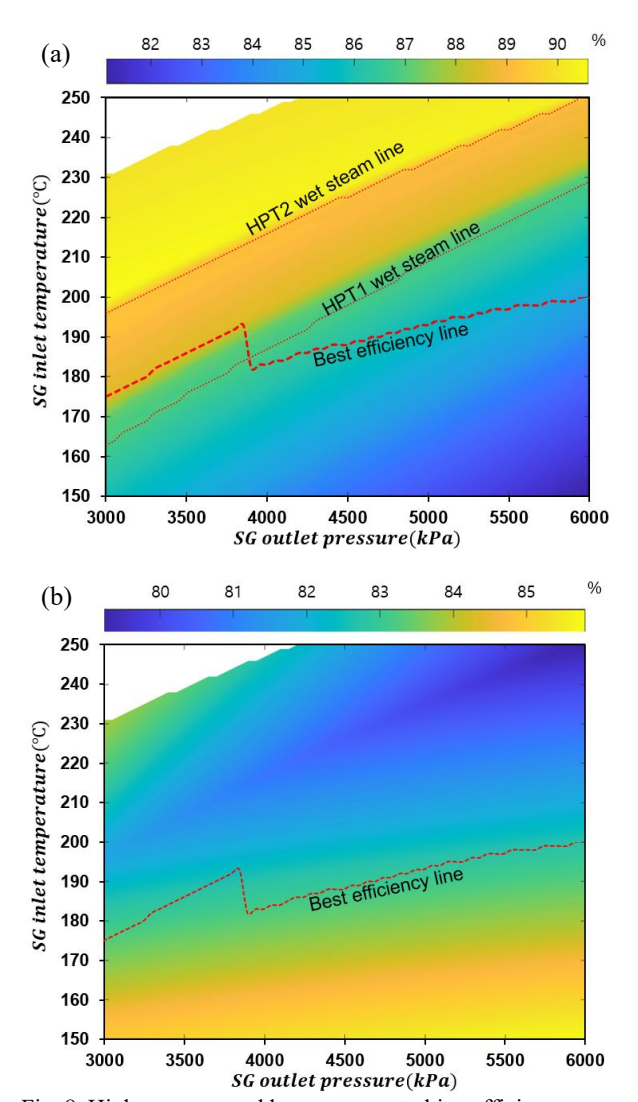


Fig. 8. High-pressure and low-pressure turbine efficiency maps under varying SG conditions: (a) HPT isentropic efficiency with wet-steam onset lines; (b) LPT efficiency in a predominantly wet region.

In Fig. 9a, the total overall heat-transfer conductance UA (sum over FWH1–FWH3; blue) is plotted along the best-efficiency locus versus SG outlet pressure: UA decreases toward lower pressure, shows a sharp local rise near ~3,800 kPa, and then declines; the orange line gives the SG inlet temperature at those same best-efficiency points. In Fig. 9b, the best net cycle efficiency is shown as a function of SG outlet pressure.

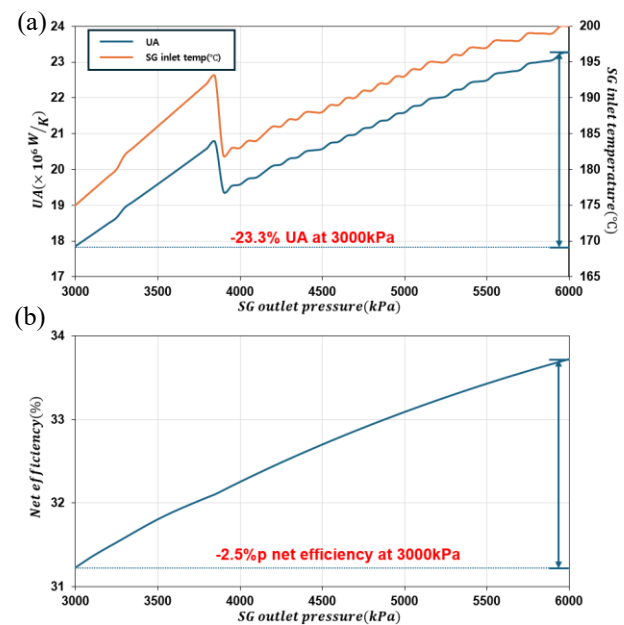


Fig. 9. (a)Total feedwater-heater UA along the best-efficiency locus by SG outlet pressure(blue) and SG inlet temperature by SG outlet pressure(orange).(b) Best efficiency by SG outlet pressure.

The SG inlet temperatures associated with those best-efficiency points are superposed and display a nearly identical inflection, underscoring the tight coupling between UA and SG inlet temperature (with fixed terminal temperature difference and drain-cooler approach, the log-mean temperature difference is effectively constant, so UA tracks heater duty).

These maps clarify the mechanisms. Raising the SG inlet temperature reduces the required HPT pressure ratio (by the FWH3 terminal constraint), which increases HPT efficiency but lowers LPT efficiency; conversely, lowering the SG inlet temperature raises the HPT pressure ratio, pushing the HPT expansion toward (or into) the wet region, where HPT efficiency changes abruptly due to moisture and supersaturation losses.

As SG outlet pressure varies, the best-efficiency path "rides" this HPT efficiency ridge: near ~4,000kPa the SG-inlet-temperature curve turns upward to avoid the HPT wet-steam penalty, producing the local spike in UA seen in Fig. 9a and the corresponding abrupt change in the best-efficiency locus in Fig. 7. Since the LPT operates predominantly in the wet region across the domain, its efficiency contributes less to the overall optimal conditions than the HPT.

Quantitatively, the difference in best net efficiency between the high-pressure and low-pressure ends of the map is only about 2.5 %p, whereas the associated difference in total UA is 23.3% (based on 6000kPa case). Thus, while the efficiency gain with higher pressure is modest, the equipment size implication is substantial—high-pressure operation demands significantly larger heat-exchange capacity.

4. Summary and Conclusions

Mapping steam-generator (SG) outlet pressure (3–6 MPa) and SG inlet temperature (150–250 °C) shows a clear trade-off between performance and equipment size. Net cycle efficiency increases with pressure, but so does the required overall heat-transfer conductance (UA) across the feedwater-heating train. Operating at the higher end of the pressure range therefore offers a modest efficiency benefit (the best-case difference is \approx 2.5%p) but entails a substantially larger UA (\approx 30.4% higher, based on 3000kPa case), implying volumetrically larger and costlier heat-exchange hardware. In addition, higher pressure pushes turbine expansions deeper into the wet-steam region; if additional moisture-removal or erosion-mitigation measures are required, overall plant size and cost can grow further.

Conversely, lower pressures reduce UA, enabling smaller, less expensive heat-exchangers, but at the expense of lower efficiency. Importantly, UA does not decrease monotonically with pressure: as pressure is reduced, there exists a localized increase in UA (observed near ~3.8 MPa) associated with a shift of the high-pressure turbine (HPT) expansion toward the wetsteam onset and the resulting redistribution of heater duty (notably into the highest-pressure feedwater heater). Designers should therefore avoid simple extrapolation and check for such non-monotonic regions when selecting operating points.

Overall, SMR secondary-side conditions should be optimized for efficiency and equipment size simultaneously, selecting SG outlet pressure and SG inlet temperature that (i) remain favorably positioned relative to the HPT wet-steam boundary and (ii) balance the marginal efficiency gain against the incremental UA (and any added moisture-management hardware). The appropriate choice will depend on project priorities—e.g., flexible, grid-responsive operation versus capital-expenditure minimization—and on site-specific constraints.

REFERENCES

- [1] U.S. DOE Office of Nuclear Energy, "Benefits of Small Modular Reactors (SMRs)"—summarizes modularity, smaller footprints, factory fabrication, and siting flexibility.
- [2] IAEA, Advances in Small Modular Reactor Technology Developments (ARIS SMR Catalogue 2024)—overview of SMR attributes including low-carbon service and modular, compact designs.
- [3] NuScale Power, Office of Technology. (2025, February 25). NuScale small modular reactor integration for hydrogen and ammonia production (WP-178373, Rev. 2)
- [4] Ingersoll, D. T., Houghton, Z. J., Bromm, R., Desportes, C., McKellar, M. G., & Boardman, R. D. (2014). NuScale small modular reactor for co-generation of electricity and water. Desalination, 340, 84–97. https://doi.org/10.1016/j.desal.2014.02.023
- [5] International Atomic Energy Agency (IAEA). (2016). Advances in small modular reactor technology developments (IAEA-TECDOC-1785). Vienna, Austria: IAEA.

- [6] Subki, I. (2011, January 12). IAEA perspective on small modular reactors (SMRs)
- [7] U.S. Nuclear Regulatory Commission. (2025, April 18). NRC begins pre-application review of Westinghouse AP300 small modular reactor.
- [8] Jingyu, C. (n.d.). Research on applying dry cooling technology in AP1000 nuclear power [Presentation]. (Notes report AP1000 main steam ≈ 5.53 MPa.) Retrieved August 15, 2025.
- [9] Lienhard, J. H., IV, & Lienhard, J. H., V. (2020). A heat transfer textbook (5th ed.). Cambridge, MA: Phlogiston Press.
- [10] Saari, J. (n.d.). Heat exchanger dimensioning [Lecture notes]. Lappeenranta University of Technology. Retrieved August 15, 2025
- [11] Towler, G., & Sinnott, R. K. (2013). Chapter 3: Utilities and energy efficient design. In Chemical engineering design: Principles, practice and economics of plant and process design (2nd ed.).
- [12] Shamoushaki, M., Niknam, P. H., Talluri, L., Manfrida, G., & Fiaschi, D. (2021). Development of cost correlations for the economic assessment of power plant equipment. Energies, 14(9), 2665. https://doi.org/10.3390/en14092665
- [13] Yong Jae Chae, Jeong Ik Lee, Thermodynamic analysis of compressed and liquid carbon dioxide energy storage system integrated with steam cycle for flexible operation of thermal power plant, Energy Conversion and Management, Volume 256, 2022, 115374, ISSN 0196-8904
- [14] EPRI, Level Control Guide for Feedwater Heaters, Moisture Separator/Reheaters, and Other Equipment, 2002, Plant Reliability and Resilience.
- [15] Spencer, R. C., k. C. Cotton, and C. N. Cannon. 1974. A Method for Predicting the Performance of Steam Turbine-Generators... 16,500 kW and Larger. Based on ASME Paper No. 62-WA-209, July 1974.